On the Ageing Behaviour of a Polyethylene Blend: Influence of Chemical Defects and Morphology on Charge Transport

S. Tantipattarakul[1,2*], A. S. Vaughan[1], T. Andritsch[1]

[1] Tony Davis High Voltage Laboratory, University of Southampton, Southampton, SO17 1BJ, United Kingdom
[2] Maintenance Division, Electricity Generating Authority of Thailand, Nonthaburi, Thailand
[*] st2f14@soton.ac.uk

Abstract: The properties of novel cable insulation systems will rely critically upon the morphology of the material. Here, a blend of high and low density polyethylene was processed in order to generate three sets of samples with different morphologies. The influence of thermo-oxidative ageing at 120 °C was then considered. The resulting chemical changes included the introduction of unsaturation and oxygen-containing groups and was determined by antioxidant consumption and oxygen permeability. Such chemical defects were found to be concentrated in the fraction of each system that was molten at 120 °C and, consequently, served to inhibit recrystallisation following ageing. The resulting spatial distribution of charge trapping sites was therefore strongly dependent on morphology. The electrical conductivity of each system varied non-monotonically with ageing: short times reduced the conductivity; a rapid increase in conductivity over five orders of magnitude occurred beyond a critical ageing threshold. Despite the pronounced structural differences between the morphologically distinct sets of samples, all exhibited comparable conductivity values beyond this threshold, implying that while charge transport is strongly influence by chemical factors, crystallinity is relatively unimportant. This experimental finding appears at odds with theoretical studies of the electronic states in crystalline and amorphous polyethylene.

1. Introduction

Although fossil fuels have played a key role in the development of the modern world, future demands for energy will need to be met through renewable sources in order to mitigate the worst effects of climate change. While a wide range of proven renewable electricity generating technologies exists, increasingly, generation locations remote from centres of energy consumption will need to be exploited, requiring massive power flows over long distances. In urban areas, in the case of subsea interconnections or where the visual impact of overhead lines is unacceptable, new cable designs will form a key enabling technology. Indeed, the Südlink project in Germany will require the installation of ~1000 km of 500 kV underground high voltage direct current (HVDC) cables to connect wind generation close to the northern seaboard to demand centres in the centre and south of the country. In total, TransnetBW GmbH has estimated that Germany will require new HVDC transmission corridors with a total length of between 2600 km and 3100 km and with a total transmission capacity of about 12 GW [1]. The reliability of the component cables will be critical in the viability of such plans.

At present, the polymer of choice for use as the insulation material in transmission cables is based upon polyethylene (PE) and, as such, understanding of the links between the composition, structure and electrical performance of PE – and how these change with time – is of enormous technological relevance. Indeed, the recent development of 525 kV and 640 kV HVDC cable designs [2, 3] derive directly from the development of novel PE molecular architectures that lead to reduced contamination levels within the final cross-linked insulation [4]. However, the processes of ageing in service will also lead to the introduction of chemical defects, which will affect properties. In the case of polyethylene, chain scission reactions lead to the formation of free radicals, which react with available oxygen to form hydroperoxides. These moieties subsequently decompose to form yet more radicals, through chain branching reactions [5, 6], and lead to the formation of ketones, esters, carboxylic acids and aldehydes [7-9]. Numerous studies of polymer ageing and its effect on the electrical behaviour of polymers have been reported. For example, it has been suggested that ageing is initiated at applied electric fields in excess of ~20 kV/mm through chain scission processes, free radical generation, the formation of submicro-cavities and the consequent accumulation of space charge [10]. This association of free volume and charge trapping is supported by complementary theoretical study [11, 12]. Elsewhere, the importance of chemical rather than structural factors has been stressed in connection with ageing. Laurent and Teyssedre [13], for example, proposed that luminescence originating from charge recombination processes can lead to local photo-oxidation. Again, associated theoretical work supports the potential relevance of ageing-related chemical changes in affecting electrical characteristics [14, 15].

Increasingly, emerging strategies for the development of new insulation systems have considered how improved properties may stem from structural modification. For example, Andersson, et al. [16] have shown that, in the case of polyethylene, the addition of as little as 1% of high density PE (HDPE) into low density PE (LDPE) results in the growth of a population of relatively thick lamellar crystals throughout the system and that this correlates with a ten-fold reduction in DC conductivity, presumably, as a consequence of inhibited charge transport through crystalline regions. Elsewhere, computational cable design studies have suggested that the desire to move to ever higher voltages and power flows will require a move away from polyethylene [17] and, for this reason, propylene-based systems are emerging as strong contenders as next generation cable insulation

systems. However, it has been shown that careful morphological control is essential, if the required mechanical flexibility is to be achieved without compromising electrical performance [18]. Optimising morphology is key.

In this investigation, we sought to extend our studies of the impact of ageing on the electrical behaviour of a blend of HDPE and LDPE by explicitly considering morphological factors. Previously [19, 20], quenching was used to suppress extensive morphological evolution; here we exploit molecular self-assembly through fractionation and segregation [21] to generate a range of different lamellar morphologies [18-20]. In concert with judicious ageing, this provides a means of precisely distributing, on a nanometre scale, those same chemical defects that in our previous work were shown markedly to influence charge transport. Specifically, here, we set out:

- To crystallise an HDPE/LDPE blend through quenching, isothermal crystallisation at 115 °C and isothermal crystallisation at 124 °C, in order to generate three very different lamellar textures.
- To subject these systems to thermo-oxidative ageing at 120 °C – that is, ageing at a temperature at which the sample will be semi-crystalline and where the dominant lamellar framework will remain as-formed, at least for the isothermally crystallised systems.
- To determine the resulting structural and chemical changes.
- To relate these effects to charge transport dynamics within each system and, thereby, consider the relative importance of chemical defects and lamellar texture on charge transport through each system.

2. Experimental

2.1. Sample Preparation and Ageing Procedure

The material systems examined in this work were composed of 20 wt.% HDPE (HD5813EA obtained from BP Chemicals) plus 80 wt.% LDPE (LD100BW obtained from Exxon Mobil). These polymers were mixed together in the melt phase in a HAAKE Polylab twin rotor R600 mixer for 20 min at 160 °C. The resulting blend was then melt pressed at 160 °C into films nominally 200 μm in thickness between sheets of polyethylene terephthalate (PET) before being subjected to one of the following thermal treatments: (i) specimens were quenched directly into water at 20 °C; (ii) specimens were isothermally crystallised from the melt at 115 °C for 60 min and then quenched as above; (iii) specimens were isothermally crystallised from the melt at 124 °C for 240 min before, again, being quenched. These thermal treatments were chosen in order to generate radically different lamellar morphologies [22].

Specimens prepared as above were thermally aged at 120 °C in air by suspending them in a fan oven (Heraeus, Kendro Laboratory Products UT6) for periods ranging from 120 h to 720 h. These conditions were determined from initial scoping experiments and were chosen such that degradation should not be limited by oxygen diffusion [23], in contrast to work reported by us elsewhere [20]. Samples prepared as above are subsequently referred to using the following general notation T/t_a, where T is indicative of the initially imposed thermal history (quenched, Q; isothermal crystallisation at 115 °C, 115I; isothermal crystallisation at 124 °C, 124I) and t_a indicates the subsequent ageing time in hours at 120 °C.

2.2. Chemical, Structural and Electrical Characterisation

Fourier transform infrared (FTIR) spectra were obtained in attenuated total reflection (ATR) mode using a Thermo Scientific Nicolet iS5 FT-IR spectrometer equipped with iD7 AR diamond crystal plates. Spectral data were acquired from 400-4000 cm^{-1} and, for each spectrum, sixteen scans were averaged at a resolution of 4 cm^{-1}. To provide a quantitative measure of the degree of oxidation, the carbonyl index (CI) was calculated using:

$$CI = {}^{A_c}\!/_{A_{ref}} \quad (1)$$

where A_c is the area under the carbonyl peak located in the range 1714-1726 cm^{-1} (C=O stretch mode) and A_{ref} is the area of the chosen reference peaks at 2915 cm^{-1} (CH_2 and CH_3 symmetric and asymmetric stretch) [9]. While the above approach provides surface-specific chemical data, our choice of ageing regime was determined with the intention of generating uniform ageing throughout the specimen thickness. To consider this, spatially resolved confocal microprobe Raman data were obtained from specimen cross-sections, using a Renishaw RM1000 Raman system (NIR 780TF diode laser; wavelength 780 nm; maximum output power 25 mW; x50 objective lens). The required cross-sections were prepared by sandwiching the relevant polyethylene film between sheets of the styrene, ethylene/butylene, styrene triblock copolymer KRATON G1650, as described elsewhere [20]. The resulting block was then microtomed at -40 °C using an RMC MT7, CR-21 cryo-ultra microtome. Raman spectra were finally obtained at locations 10 μm apart from 500 cm^{-1} to 3200 cm^{-1}, using 10 consecutive 10 s extended scans at 50% laser power. Raw spectra were numerically processed, using the *Origin* software package, to remove background scattering and, finally, were normalised with respect to the Raman peak at 1295 cm^{-1} (C-C twisting mode) [24]. Carbonyl index values were again calculated for each acquisition point, taking A_{ref} as the area under the Raman peaks located around 2850 cm^{-1} (CH_2 and CH_3 symmetric and asymmetric stretch) and A_c as the area under the carbonyl peak at 1720±5 cm^{-1} (C=O stretch mode) [24, 25].

Sample melting behaviour was determined by different scanning calorimetry (DSC), using a Perkin Elmer DSC7 running Pyris software. All data were acquired from 40 °C to 170 °C at a scan rate of 10 °C/min, after calibration of the DSC with high-purity indium. Subsequently, the acquired data were numerically processed (normalised and slope corrected), again, using *Origin* software. Complementary real-space morphological information was obtained by scanning electron microscopy (SEM) following permanganic etching of cross-sections, prepared as described above. Samples were etched for 60 min, in line with published procedures [26], using a reagent composed of 1% potassium permanganate dissolved in an acid mixture containing 10 parts concentrated sulphuric acid, 4 parts orthophosphoric acid and 1 part water. After recovery, the

etched surfaces were sputter coated with gold and examined in an EVOLS25 Zeiss SEM.

DC conductivity measurements were used to examine the effects of sample morphology and the imposed ageing on charge transport, using a protocol in line with the ASTM D257 standard [27]. All samples were coated with gold, sputtered onto both surfaces as conductive electrodes. Measured data were acquired at 20 °C and an applied electric field of 40 kV mm^{-1} at intervals of 10 s over a period of 10000 s, using A Keithley 6487 picoammeter.

3. Results

3.1. The Influence of Ageing on Surface Chemistry

Fig. 1 shows infrared spectral data acquired from quenched samples after ageing at 120 °C for times ranging from 0 to 720 h. From this, it is evident that the chemical composition is significantly changed for ageing times in excess of 144 h, as evinced by greatly increased infrared absorbance within the ranges 800-1500 cm^{-1} and 1500-1900 cm^{-1}. Within the 800-1500 cm^{-1} range, the absorption bands are assigned to various vibrational modes associated with vinyl and vinylidene (980-955 cm^{-1}), alcohols (1096 cm^{-1}), esters (1264 cm^{-1}) and ethers (1170 cm^{-1}). The generation of these groups is related to auto-oxidation reactions, which can lead to cross-linking during ageing. Meanwhile, the absorption bands within the range1500-1900 cm^{-1} are related to carbonyl groups associated with ketone, aldehyde and γ-lactone, which are, respectively, located at 1716, 1725 and 1780 cm^{-1}. These ageing-induced chemical modifications are consistent with complementary results obtained from the same system after ageing at 160 °C; previously, we reported a marked increase in the intensity of the above bands for ageing times in excess of 3 h at 160 °C [20]. For ageing at 120 °C, comparable effects occur beyond 144 h. This suggests that increasing the temperature by 10 °C results in a reduction in the induction time of ~60%; previously, Anandakumaran and Stonkus [28] considered the behaviour of cross-linked polyethylene (XLPE) aged at temperatures from 120 to 140 °C and reported that an increase in ageing temperature of 10 °C reduced the induction time by ~50%. Fig. 2 contains equivalent infrared data obtained after

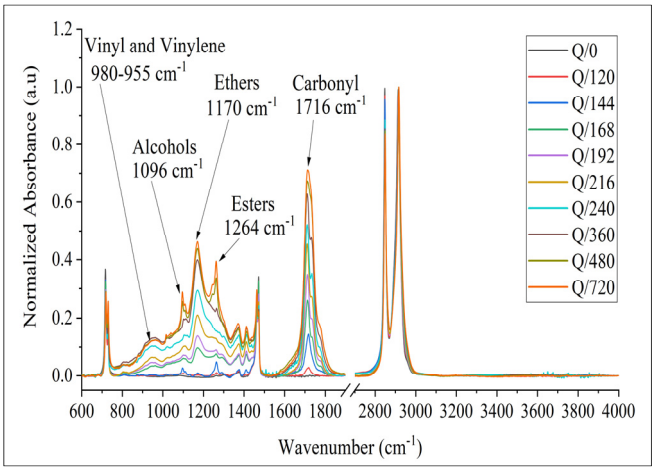

Fig. 1. *Infrared spectra obtained from quenched samples aged at 120 °C for periods ranging from 0 to 720 h.*

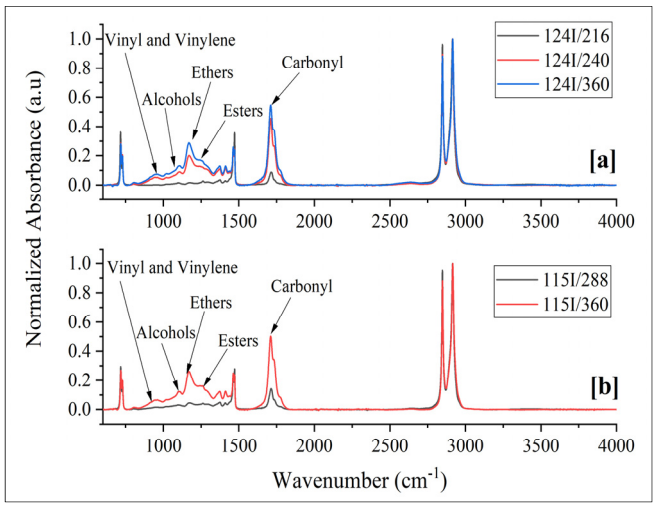

Fig. 2. *Representative infrared spectra obtained from samples aged at 120 °C for periods around the threshold ageing time: (a) 124I/t_a; (b) 115I/t_a.*

selected ageing times, from samples previously crystallised isothermally at 124 °C and 115 °C. While these spectra contain similar features to those describe above, it is also evident that the kinetics is strongly dependent on the material's thermal history, such that pronounced increases in the concentration of ageing-related products occur beyond 216 h and 288 h for the 124I/t_a and 115I/t_a sample sets respectively.

To provide a concise representation of the time dependence of thermo-oxidative degradation, the CI was evaluate for each specimen; the resulting data are plotted in Fig. 3, where the error bars represent the standard deviation derived from repeat measurements from three different samples. From this, it is evident that the ageing response of the three systems is very different but, in all cases, for ageing times less the threshold value at which a marked increase in CI occurs, CI remains close to zero. Thereafter, CI increases rapidly to a high value (CI ≈ 0.8) before remaining constant or only increasing slowly for ageing times from 360 h to 720 h. Specifically, all trends exhibit sigmoidal characteristics, which aligns with the classical pattern of induction, autoxidation and termination [5, 29]. From CI

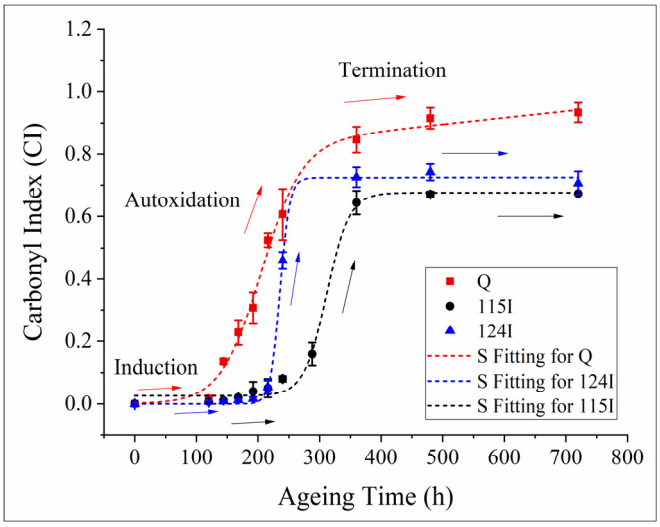

Fig. 3. *Variations in carbonyl index of Q/t_a, 124I/t_a and 115I/t_a samples aged with from 0 to 720 h.*

Table 1 The estimated parameters obtained from the fitting of CI plots

Fitting parameters	Q	124I	115I
Ageing threshold time, t_{at} (h)	107	200	240
The increasing rate of oxidation (ΔCI h^{-1})	0.004	0.010	0.005

plots, estimates of the ageing threshold time, t_{at}, and the subsequent rate of increase in the degree of oxidation can be obtained by fitting each data set to the usual Sigmoidal-Boltzmann function [30]; derived parameter values are presented in Table 1. From Table 1, t_{at} varies in the order, 115I > 124I > Q, while the subsequent rate of oxidation is ordered 124I > 115I > Q. Both of the base polymers used in this study were commercial materials and would, therefore, be expected to include antioxidants. While, in some samples, it was possible to detect the presence of the antioxidant in the FTIR spectrum the associated peaks, where detectable, were very weak; no precise identification was therefore possible, beyond saying that they appear to be related to a phenolic antioxidant. As such, as reported elsewhere, we associate the initial induction period with consumption of the included antioxidant [5, 29]. All these systems were prepared from the same starting materials and, therefore, should contain the same antioxidant content and the same molecular composition. However, the crystallisation conditions were deliberately chosen in order to generate materials with different morphologies and, therefore, we suggest that the differences in ageing parameters listed in Table 1 are morphological in origin.

3.2. Ageing in The Bulk

Fig. 4 shows Raman spectra acquired from the cross-section of Q/216. The data were measured at nineteen positions at a separation of 10 µm, starting from ~10 µm beneath the sample surface. Here, it is evident that the Raman scattering varies very little through the sample thickness, indicating a uniform chemical composition. This is markedly different from the behaviour reported in our previous work [19, 20], where the ageing conditions were deliberately chosen to lead to oxygen diffusion limited degradation. The spectra shown in Fig. 4 evince the same chemical groups as seen previously, namely alcohols (871 cm^{-1}), unsaturation

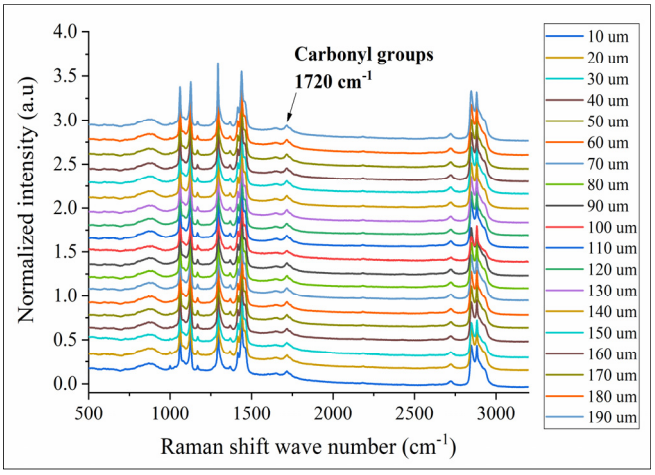

Fig. 4. *Raman spectra obtained from the indicated cross-sectional position within specimen Q/216.*

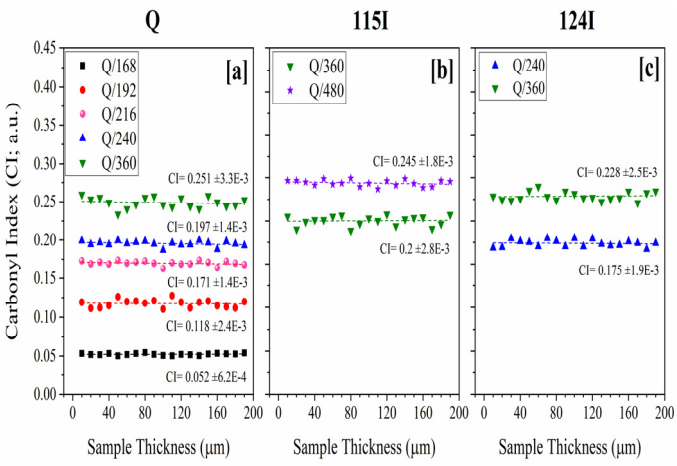

Fig. 5. *Variations in carbonyl index with cross-sectional position through representative specimens: (a) Q/t_a; (b) 115I/t_a; (c) 124I/t_a.*

(1618 cm^{-1}) and carbonyl groups (1720 cm^{-1}). To illustrate the spatial variation in the degree of ageing, the same general procedure as used in Fig. 3 was employed and the resulting variation in CI as a function of position is shown in Fig. 5 for selected samples. The rationale behind this choice of aged samples is based both on instrumental limitations and on the differences between the fundamental mechanisms inherent in Raman and FTIR spectroscopy [24]. Here, the strength of Raman carbonyl bands could not be reliably evaluated for systems where the FTIR CI value was less than ~0.2. Furthermore, Raman data obtained from severely aged samples (t_a > 360 h) could not be analysed because the resulting spectra were swamped by fluorescence, despite the use of a near-infra red excitation laser [31].

Comparison of Figs. 3 and 5 demonstrates that CI values obtained from Raman spectroscopy are, numerically, lower than those obtained from FTIR. For example, Q/192 is characterised by an FTIR CI value of 0.307 ± 0.05 and Raman CI values of 0.118 ± 0.002. Nevertheless, the Raman data shown in Fig. 5 reveal, in all systems, increasing CI values with increasing ageing time and, more significantly given the objectives of this work, a uniform distribution of oxidation across the sample thickness. That is, as anticipated, the chosen ageing protocol is such that the rate of diffusion of oxygen into the material is greater than its internal rate of consumption.

3.3. Ageing and Lamellar Texture

Fig. 6 shows DSC melting data obtained from samples aged for different periods at 120 °C. Consider, first, results obtained from samples prepared by quenching from the melt. Here, the melting behaviour of the unaged reference system is characterised by a broad melting endotherm spanning the range ~60 – 125 °C, which can be discussed in terms of the three features (arrowed), located at 101 °C (low temperature feature), 115 °C (intermediate temperature feature) and 124 °C (high temperature feature).

Previous analyses [22, 32] have interpreted comparable melting behaviour in HDPE/LDPE blends as follows: the low temperature feature results, primarily, from the melting of the majority, low density component of the blend; the intermediate feature, in the case of some

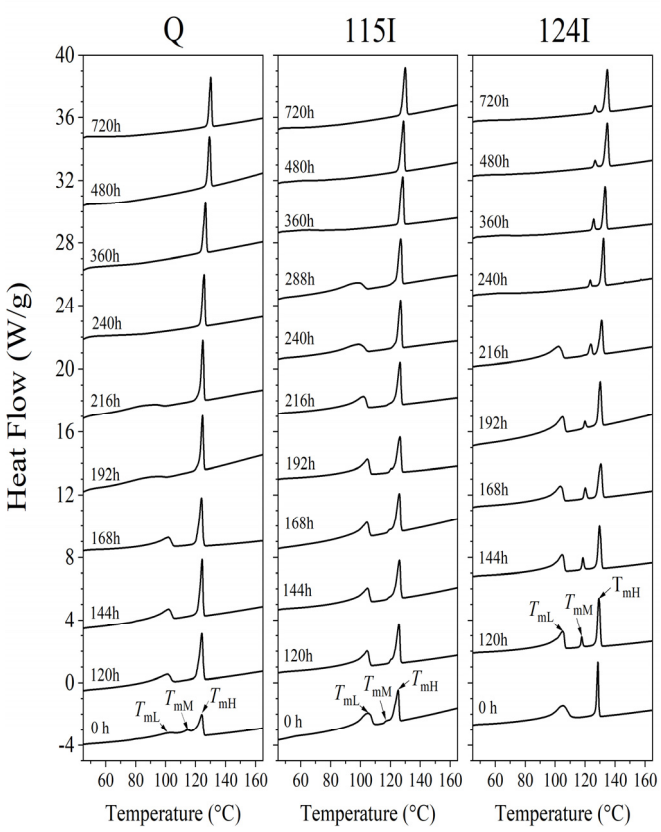

Fig. 6. *DSC melting data obtained from samples aged for the indicated times after quenching (Q), isothermal crystallisation at 115 °C (115I) or isothermal crystallisation at 124 °C (124I). Indicated temperatures are, from left to right T_{mL}, T_{mM} and T_{mH}*

isothermally crystallised PE blends, has previously been associated with a lamellar population resulting from co-crystallisation of HDPE and the more crystallisable components (i.e. linear chain segments) within the LDPE; the highest melting peak is then related to crystals containing only HDPE. However, examination of the melting endotherm of the sample aged for 120 h demonstrates that this attribution is incorrect here. The fact that the melting behaviour of the Q/120 sample involves just two components (peak melting temperatures of 101 °C and 124 °C) demonstrates that annealing (at 120 °C) can result in reorganisation of the intermediate-melting lamellar fraction and, as a result of this, the highest melting component of Q/120 appears increased in size compared with that of Q/0. As such, we suggest that the measured melting behaviour of Q/0 is a consequence of both the initial lamellar population, which formed rapidly on quenching, and subsequent annealing and reorganisation of this during the course of the DSC scan, as seen elsewhere [33]. Further ageing, up to 168 h, has little effect, but thereafter, the magnitude of the lower temperature melting endotherm is progressively reduced, such that for ageing times of 240 h and above, only the higher temperature peak is evident.

Samples produced by isothermal crystallisation at 115 °C behave in a comparable manner, albeit that the chosen thermal history renders this system less prone to reorganisation in the DSC, such that the melting traces obtained from the 115I/0 and 115I/120 samples are broadly equivalent. While prolonged ageing, again, results in eradication of the lower melting feature, in these systems, this requires a longer ageing period than for the quenched systems discussed above. In the case of samples crystallised isothermally at 124 °C, the melting endotherm of the unaged reference system is composed of two components; the higher melting feature contains the most crystallisable components of the blend (formed at 124 °C and derived from the HDPE), while the lower melting feature is related, *primarily*, to the LDPE. However, the emergence of the small intermediate peak, at temperatures ranging from 118 °C (124I/120) to 127 °C (124I/720) reinforces previous assertions [34] that isothermal crystallisation of such PE blends above ~120 °C may result in rejection of low molar mass HDPE fractions from the advancing crystal/melt interface into the predominantly LDPE melt. Here, prolonged annealing at 120 °C would appear to be sufficient to facilitate crystallisation of this fraction, which was previously rejected during the initial crystallisation step at 124 °C.

Fig. 7 presents a quantitative evaluation of the effect of ageing time on overall sample crystallinity [5], based on the melting traces shown in Fig. 6; the error bars shown represent the standard deviation derived from repeat measurements from three different samples. While the initial effect of ageing at 120 °C is to increase the crystallinity, the crystallinity then drops over a period that is strongly dependent upon the initial crystallisation conditions – this occurs after notably longer ageing times in the case of the 115I/t_a sample set. Thereafter, crystallinity varies only weakly. Comparison of Figs. 3 and 7 reveals clear parallels. In the case of samples initially crystallised isothermally at 124 °C, for example, the induction process, as deduced from the CI data, leads to t_{at} = 200 h; the carbonyl index then increases rapidly over the next 50 h of ageing before saturating. The crystallinity, similarly remains close to constant up to t_a = ~200 h, before decreasing rapidly up to t_a = ~250 h. Similar parallels can be drawn between Figs. 3 and 7 for the specimens prepared by quenching and isothermal crystallisation at 115 °C. However, it is notable that, both in terms of variations in CI and crystallinity, isothermal crystallisation at 115 °C results in a material that exhibits a marked increase in resistance to degradation.

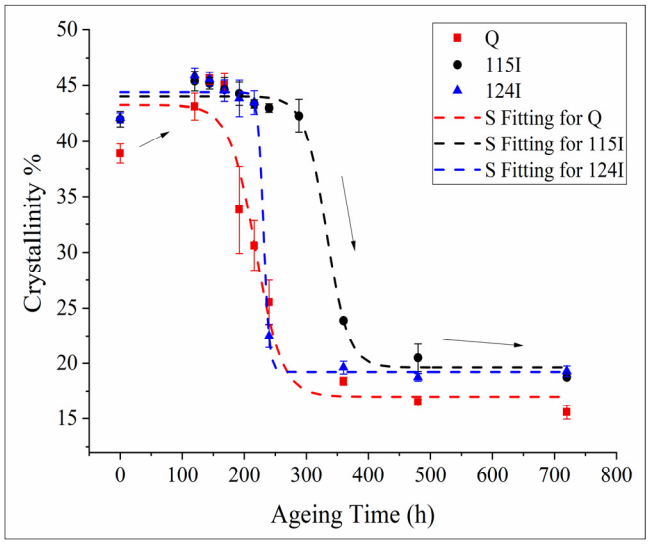

Fig. 7. *Effect of thermo-oxidative ageing at 120 °C on the total DSC crystallinity of samples prepared by after quenching (Q), isothermal crystallisation at 115 °C (115I) and isothermal crystallisation at 124 °C (124I).*

The effect on PE of ageing in the presence of oxygen has been considered by many workers. Recently, Li, et al. [35] considered thermo-oxidative ageing of XLPE in the temperature range 100-160 °C – that is, both above and below the peak melting temperature of the unaged system (~108 °C). This work concluded that oxidation occurs predominantly in the non-crystalline regions and that the induction time is related to consumption of antioxidant; as such, a key factor relates to oxygen diffusion through the system, which is strongly dependent on crystallinity [36, 37]. However, the very different induction times seen in Q/t_a and 115/t_a systems, despite their comparable crystallinity levels, demonstrates that crystallinity, *per se*, is an insufficient metric. While we are unaware of any direct studies of the influence of specific morphologies, as opposed to gross crystallinity, on oxygen diffusion through PE, various related aspects of the problem have been addressed. Mattozzi, et al. [36], for example, contrasted linear and branched polyethylene, and considered the reduction of crystallinity of the latter as leading to an increased penetrable fraction; Chmelař, et al. [38], highlighted the importance of the spatial distribution of the amorphous and crystalline phases in penetrant diffusion.

To conclude, we suggest the behaviour presented above can be interpreted as follows:

(i) Initially, the crystallinity increases, as a result of annealing effects, which are enhanced by chain scission reactions in amorphous/molten regions, as proposed by Khabbaz, et al. [39] and Anandakumaran and Stonkus [28].

(ii) The subsequent marked decrease in crystallinity occurs after the oxidation induction phase is complete, which corresponds to consumption of the antioxidant [5, 29, 35]. The duration of this is governed by the rate of diffusion of oxygen into the material, which itself is determined by both the penetrable fraction (i.e. the fraction of system in the amorphous/melt phase) and its spatial distribution (i.e. the tortuosity of the diffusion path).

(iii) After induction, degradation occurs primarily within the amorphous/melt (i.e. outside crystalline lamellar cores), such that the resulting chemical defects (e.g. carbonyl groups) and modified molecular topologies (gel content) serve greatly to limit the scope for subsequent recrystallisation of the affected material on termination of ageing.

(iv) The final phase, where, the crystallinity varies only weakly with ageing time, is related to the much slower degradation of that component of the system that remains in the solid state throughout the ageing period. This higher melting lamellar fraction appears relatively resistant to thermo-oxidative ageing under the conditions used here.

3.4. Ageing and Sample Morphology

Fig. 8 contains three SEM micrographs showing the effect of ageing on the morphology of samples prepared initially by quenching from the melt. From Fig. 8a, it is evident that the morphology of this unaged reference system is based upon spherulites, ~5 µm in diameter and with a band period of ~400 nm. After ageing at 120 °C for 168 h (see Fig. 8b), the morphology appears rather coarser; the spherulites appear somewhat larger, while the band period is markedly increased to ~1.3 µm [40]. From Fig. 6, the DSC melting endotherm of Q/168 contains a low temperature peak at 102 °C (i.e. below the ageing temperature), which must therefore correspond to a lamellar population that formed on quenching at the end of the ageing period. In addition, the higher melting peak is markedly sharper and more pronounced compared with the equivalent feature in the unaged reference system. As such, the morphology described above is consistent with the DSC data whereby, during the

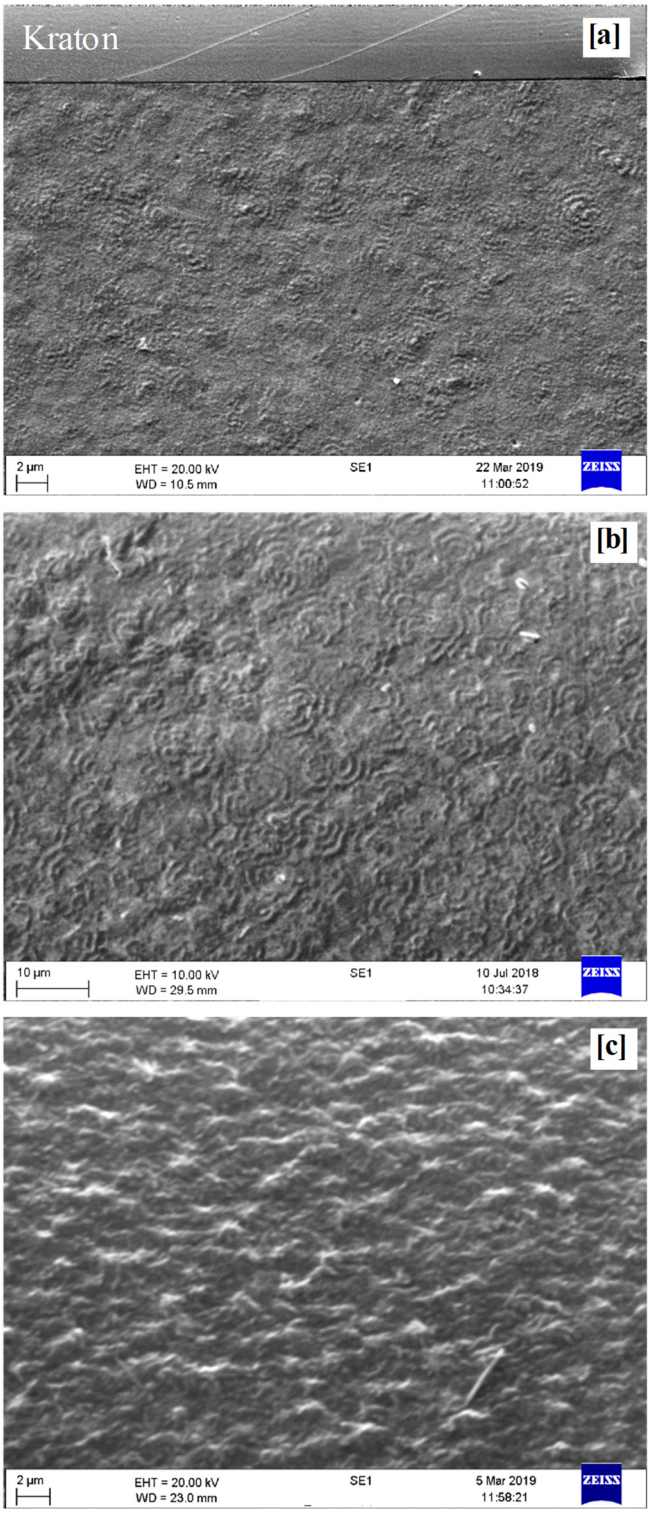

Fig. 8. *SEM micrographs showing the morphology of etched cross-sections in quenched samples aged as follows: (a) unaged reference; (b) aged at 120 °C for 168 h; (c) aged at 120 °C for 360 h.*

induction period, the ageing processes' dominant effect is to anneal the system. However, ageing for longer times leads to a change in the surface texture (see Fig. 8c, which shows a sample aged for 360 h). From Fig. 6, ageing for periods greater than 216 h results in the elimination of the lower melting peak. That is, this thermo-oxidative treatment is sufficiently severe as to introduce enough defects (chemical groups and crosslinks) to prevent the melt from recrystallising when the ageing period is complete; the remnant lamellae are then separated by highly defective, amorphous regions. The essence of the permanganic etching technique, as described by Olley [41], is that the rate of removal of molecular fragments is determined by local ordering and defect content and, in this context, the kinetics of the process will be greatly increased in the case of quenched amorphous regions (as in Q/360) compared with quenched semi-crystalline regions (as in Q/168). Comparable examples of the etching behaviour of defective systems can be found in the literature [42]. As such, we suggest that the difference in the surface texture seen in Fig. 8c, compared with both Figs. 8a and 8b, is an etching effect and is directly related to the absence of the low melting endotherm in the DSC melting behaviour of Q/360 seen in Fig. 6.

Equivalent morphological data to those discussed above, but obtained from samples initially crystallised isothermally at 115 °C, are presented in Fig. 9. In line with published work [32, 43], the morphology shown equates to a space-filling arrangement of banded spherulites, where the band period (~2 μm) is increased significantly compared with that seen in Fig. 8, as a result of the spherulites having formed at 115 °C [44]. This texture is based upon individual lamellar crystals that developed isothermally at 115 °C (melting endotherm >115 °C in Fig. 6), separated from one another by quenched material (melting endotherm <110 °C in Fig. 6). Fig. 9b shows the morphology of a sample after ageing for 288 h; from Fig. 6, this system still exhibits a broad low melting peak together with a sharp peak at 127 °C, the latter corresponding to the annealed, isothermally crystallised, lamellar fraction. That is, the DSC melting behaviour of 115I/0 and 115I/288 are comparable and, therefore, it is unsurprising that the morphologies shown in Figs. 9a and 9b are also well-aligned. In Fig. 9c, further ageing (for 360 h) can be seen to lead to a marked change in the texture of the etched surface. As in the above discussion of the quenched specimens, this ageing time is sufficient to prevent recrystallisation of the molten components on quenching at the end of the imposed ageing period and, therefore, the isothermally formed lamellar fraction, which remained in the solid state throughout, would then be separated by amorphous regions. As proposed above, this amorphous fraction is readily etched, to give the porous surface appearance shown. Finally, Fig. 9 provides an explanation for the extended induction time seen in samples isothermally crystallised at 115 °C; the space-filling array of lamellar crystals results in a great increase in the tortuosity of the diffusion path (through intervening amorphous/melt regions), thereby, slowing the effective rate of oxygen diffusion into the system.

Fig. 10, finally, shows the morphology of systems initially crystallised at 124 °C. In the sample 124I/0 (see Fig. 10a), isolated, dense aggregates of isothermally crystallised lamellae can be seen dispersed within a continuous, quenched phase, which is devoid of structural detail at this

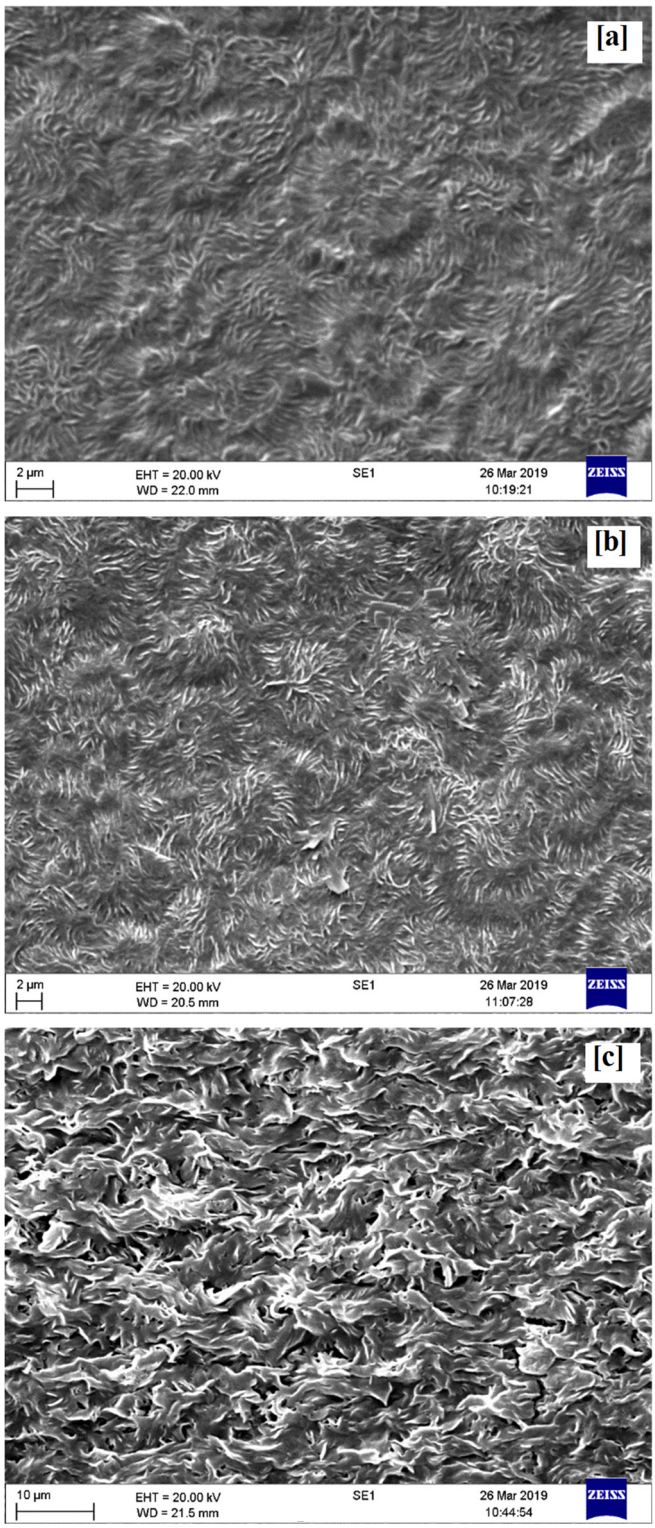

Fig. 9. *SEM micrographs showing the morphology of etched cross-sections in isothermally crystallised (115 °C) samples aged as follows: (a) unaged reference; (b) aged at 120 °C for 288 h; (c) aged at 120 °C for 360 h.*

magnification [32]. These two morphological elements correspond, respectively, to the sharp peak at 128.5 °C and the broad peak at 105 °C in the DSC melting endotherm of the unaged specimen (see Fig. 6). The morphology of a sample aged at 120 °C for 216 h is shown in Fig. 10b, from which, is evident that while such a thermal treatment appears to have relatively little effect on the isothermal lamellar

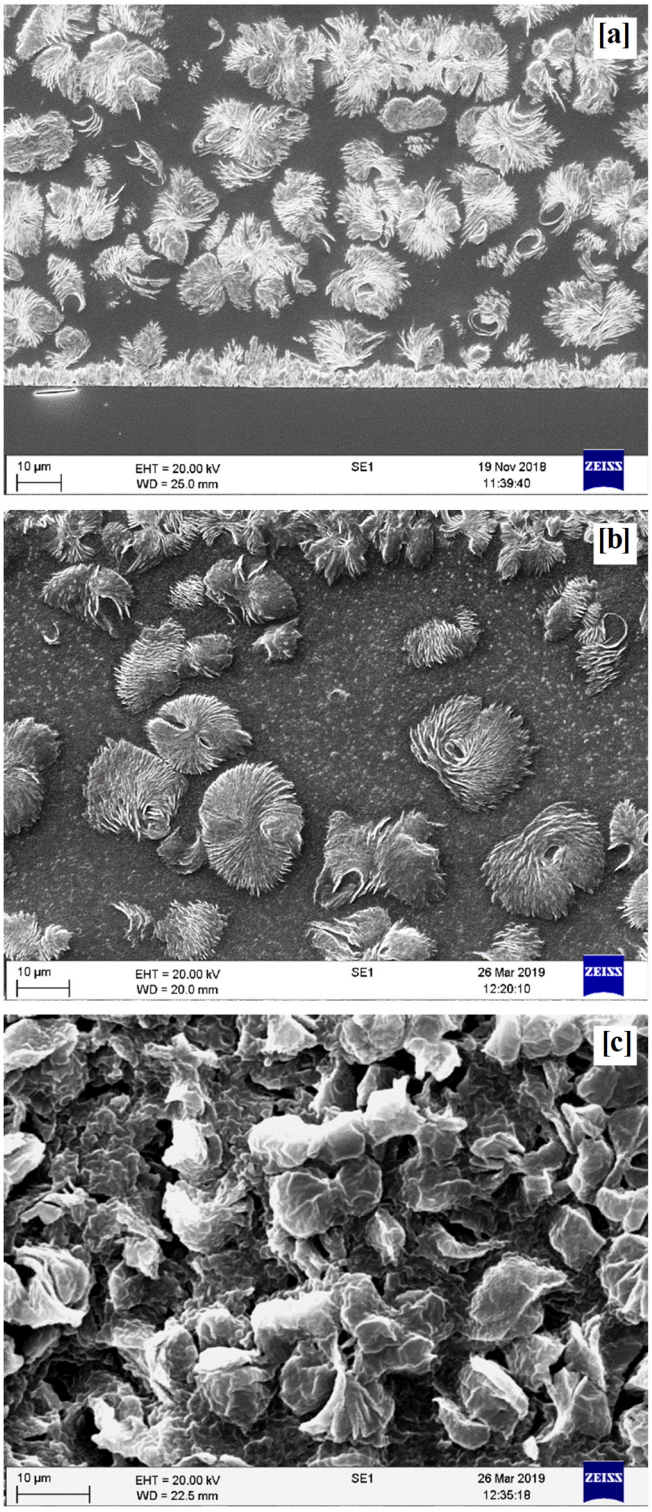

Fig. 10. *SEM micrographs showing the morphology of etched cross-sections in isothermally crystallised (124 °C) samples aged as follows: (a) unaged reference; (b) aged at 120 °C for 216 h; (c) aged at 120 °C for 360 h.*

aggregates, now, the quenched matrix contains enhanced structural detail, which we relate to the small, intermediate melting peak arrowed in the melting trace of this system in Fig. 6. The effect of further ageing, to beyond the point at which recrystallisation of the melt is prevented, again results in accelerated removal of the now amorphous quenched material on etching, resulting in the greatly roughened surface appearance of Fig. 10c.

In summary, the DSC and SEM data obtained are consistent and complementary and the morphological differences account for the variation in oxidation induction time shown in Fig. 3. The as-formed morphologies seen here are in line with expectations based upon previous reports [22, 32, 43]. The chosen ageing temperature of 120 °C serves to anneal the components of the system that are crystalline at this temperature and, beyond the threshold time, to introduce defects into the amorphous/melt components. While these effects are amplified by the molecular composition, imposed crystallisation conditions and chosen ageing temperature, the consistency of the effects and the alignment with complementary published work suggest that, at least at temperatures above the glass transition, the principles articulated apply to all semi-crystalline polymers which, by definition, contain both crystalline and mobile amorphous regions.

4. Ageing, Morphology and Charge Transport

Fig. 11 presents representative time dependent conductivity data obtained from various 115I/t_a samples. From this, it is evident that the current flowing through each specimen, initially, drops significantly over a period that varies from sample-to-sample before approaching steady state, as widely reported [45-47]. In seeking to estimate a DC conductivity value from such data, a number of strategies are possible, such as averaging a number of current measurements obtained within the apparently steady state regime, or fitting the raw data to some suitable function. Recently, Hosier, et al. [48] contrasted these two approaches and reported that, for their systems, the use of the Curie von Schweidler law [49] modified by the addition of a time-independent steady state DC conduction term led to more reliable DC conductivity values. As such, the same approach was used here but, in this case, the results were found to fall within the uncertainties associated with direct current measurements. As such, all evaluations of material

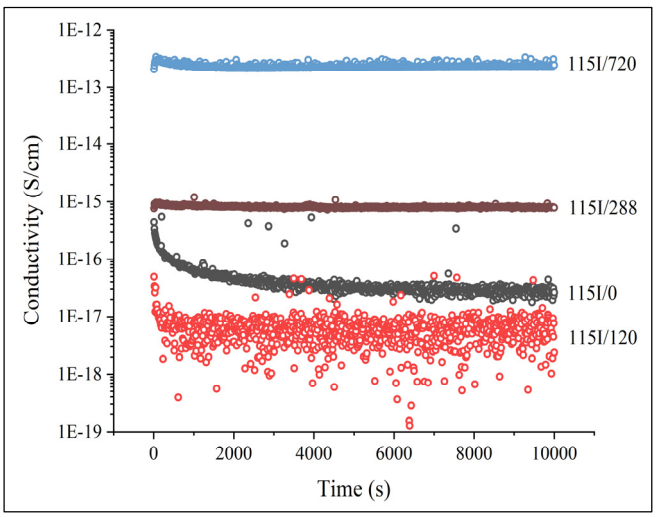

Fig. 11. *The time dependence of DC conductivity of 115I samples with indicated ageing times, which the magnitude values as a function of time are plotted in log-linear scale.*

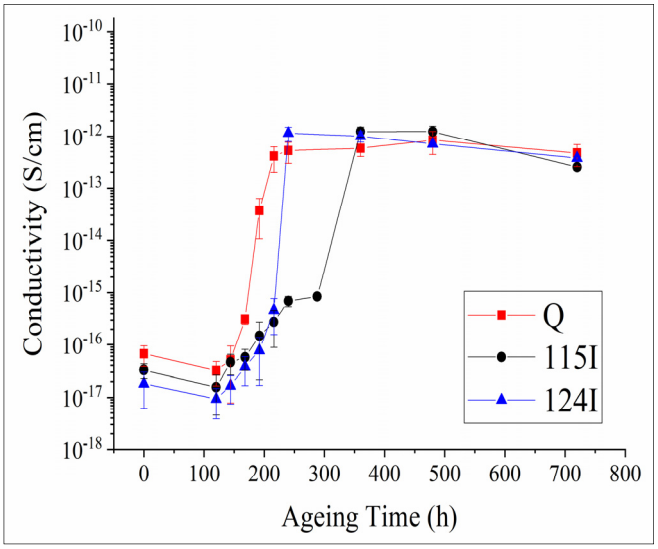

Fig. 12. *The quasi-steady state values of conductivity of all morphologically distinct samples aged from 0 to 720 h, obtained at 20 °C and 40 kV mm^{-1} of the applied voltage.*

conductivity are based upon current measurements made 9,900 s to 10,000 s after application of the voltage.

Fig. 12 shows the effect of ageing on conductivity, σ, for the three morphologically distinct sample sets considered here; the error bars shown represent the standard deviation derived from repeat measurements from three different samples. Initially, the conductivity falls somewhat, for ageing times up to 144 h at 120 °C; this parallels previous work concerning the effect of ageing at 160 °C [20] and the work of Karlsson, et al. [50], where an initial reduction in conductivity was also seen. This phenomenon can arise through to two processes, both of which stem from the introduction of a low concentration of deep traps into the system. First, the presence of deep traps near the electrodes will result in the formation of homocharge, which will serve to reduce the interfacial electric field and, thereby, inhibit further charge injection. Second, the presence of a low concentration of deep traps will, according to space charge limited conduction, serve to reduce the effective charge carrier mobility. Beyond a threshold ageing time, the conductivity increases at a rate that is dependent upon the system, to a saturation value that in all cases is close to 10^{-12} S/cm. In discussing this, it is pertinent to consider three factors: overall crystallinity; morphology (i.e. the spatial distribution of the crystalline phase); chemical changes.

Comparison of Figs. 12 and 7 reveals a clear anti-correlation between the $\log_{10}\sigma$ and the measured crystallinity. Consider, for example, the 115I/t_a sample set. Initially, the crystallinity increases to ~46 % for ageing times up to ~144 h; the measured conductivity falls from 3.31×10^{-17} S/cm to 1.56×10^{-17} S/cm over the ageing period 0 – 120 h. The crystallinity then falls slowly from 144 h to 300 h; the conductivity increases from 1.56×10^{-17} S/cm to 8.39×10^{-16} S/cm over the same ageing period. Next, the crystallinity decreases (from ~42% at 288 h to ~23% at 360 h); the conductivity increases by around three orders of magnitude over this same ageing period. Finally, both the crystallinity and conductivity remain close to constant up to the longest ageing time considered here. Similar correlations can also be seen for the Q/t_a and 124I/t_a systems.

Charge transport in PE has been considered, theoretically, in numerous studies. Early approaches to the evaluation of the band structure of polymers considered these as idealised, infinite, regular systems; in their 1971 paper, McAloon and Perkins [51], for example, contrasted the application of a linear combination of atomic orbitals molecular orbital approach with alternative published work and proposed a band gap for PE of around 19 eV: a value that is unreasonably large. The influence of the theoretical approach on the calculated band gap of a single, infinite polymer chain was discussed by Süle, et al. [52], where band gap energies ranging from 4.4 eV to 9.7 eV were reported, depending on the methodology used. A natural extension to such work is to consider a perfect crystal; Cubero, et al. [12] calculated the excess electron states in the linear alkane $C_{27}H_{56}$, demonstrating that the electron affinity is negative, as in PE. However, when the finite alkane crystal thickness was taken into account, the bottom of the conduction band was found to correspond to interlayer states, rather than the interchain states of crystalline PE. The impact of structural factors on the electronic structure of PE was considered by Moyassari, et al. [53], where band gap energy values of 6.00 eV, 6.73 eV and 5.89 eV were reported for amorphous, crystalline and interfacial structures respectively. Elsewhere, combinations of molecular dynamics and density functional theory have indicated that, in amorphous PE and related analogues, conformational defects lead to electron traps, with energies ~0.15 – 0.5 eV below the vacuum level [12, 53, 54]. Subsequent work by the same group extended such ideas, concluding that the introduction of an excess electron into PE could result in the formation of a self-trapped polaron centred on a small cavity-like region within the structure [55].

Considering the variations in conductivity and crystallinity presented above in concert with the body of theoretical work in the literature, it is tempting to conclude that, at least as far as electrons are concerned, charge transport through crystalline polyethylene is not favoured which, initially, appears consistent with the experimental results presented above. This, however, fails to consider morphological factors. Comparison of Figs. 8, 9 and 10 reveals very different spatial distributions of crystals in the three systems and, taken together with the DSC data presented in Fig. 6, it is evident that the thickest and most perfect lamellae remain intact up to the maximum ageing time considered here. Contrast, for example, the two isothermally crystallised systems when aged for 360 h. In the case of 124I/360, the morphology is then based upon *discrete* crystalline aggregates (overall crystallinity ~20%) that are separated from one another by a *continuous* amorphous phase; conductivity 9.97×10^{-13} S/cm. In marked contrast, 115I/360 is characterised by comparable overall crystallinity (~23%) and conductivity (1.23×10^{-12} S/cm) values, but in this system, it is the crystalline phase that can be considered as a largely *continuous* array of crystalline structures, separated from one another by *discrete* amorphous regions. While the absolute connectivity of the amorphous phase in 115I/360 cannot be ascertained categorically from the available structural information, the *prima facie* evidence strongly suggests that any percolating pathways through 115I/360 will be very much longer and more tortuous than in 124I/360; experimental support for this is provided by the reduced effective diffusion rate of oxygen through amorphous regions

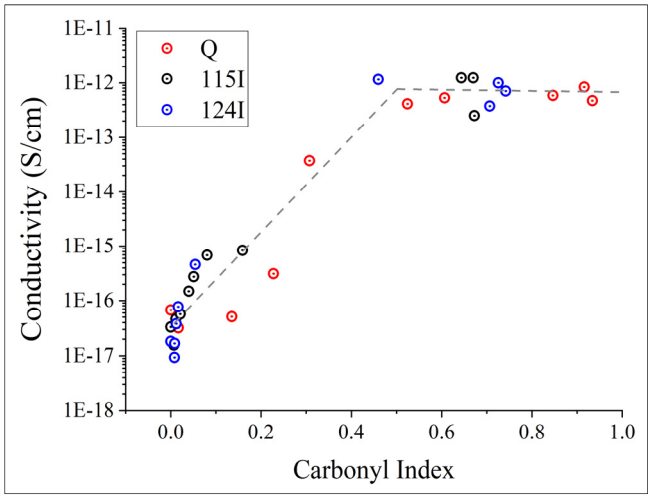

Fig. 13. *The plots of quasi-steady state values of conductivity of all morphologically distinct samples aged from 0 to 720 h, as a function of carbonyl index.*

in the 115I/t_a specimens. Despite this, the conductivity of 115I/360 and 124I/360 is equivalent.

The relationships between CI and crystallinity and crystallinity and conductivity have been discussed separately above and, therefore, for the sake of brevity, only the key features relating CI and conductivity will be stressed here. Comparison of Figs 3 and 12 demonstrates clear parallels between the variation with ageing time of CI and $\log_{10}\sigma$. Initially, both parameters vary only weakly with ageing; both then increase markedly before reaching approximately constant values. Generally, the marked increase in CI and $\log_{10}\sigma$ occurs first for Q/t_a, then for 124I/t_a and, finally, for 115I/t_a. Since sample chemistry and conductivity appear well correlated, conductivity is plotted against CI in Fig. 13. From this, it is evident that the data are broadly clustered into two groups: systems characterised by CI values less than about 0.2 and a conductivity in the range 10^{-17} – 10^{-15} S/cm; systems characterised by CI values greater than 0.4 and a conductivity close to 10^{-12} S/cm. This is consistent with our previous observation of a marked and sudden increase in conductivity on exceeding a critical ageing time [20], whereupon, discrete deep traps, when present above a critical concentration, facilitate conduction. The invariant conductivity seen in samples aged such that CI > 0.4 is also consistent with such process, whereby increase of the density of traps facilitates a percolation processes. This effect of ageing at 120 °C on the traps present in XLPE has been considered by Boukezzi et al. [56], who estimated a resultant trap depth of 0.8 – 0.9 eV based upon their thermal stimulated current measurements.

5. Conclusions

In the work described above, three different morphologies were generated in a polyethylene system of constant composition, through a judicious choice of molecular components and imposed thermal history. These were subsequently aged under conditions (at 120 °C in air) whereby the essential morphological differences were preserved, but a range of molecular defects was introduced into each system in specific structural locations. Although the kinetics of ageing were markedly slowed compared to our previous work, where ageing of the same system was conducted at 160 °C, otherwise, the defects introduced into the molten fraction of each system appear equivalent. The lamellar fraction that remained in the solid state throughout was largely immune to ageing, presumably because defect formation was concentrated at basal fold surfaces. Previously, we reported that an abrupt change in charge transport dynamics occurred when the same blend system was aged at 160 °C and associated this with the establishment of a critical density of charge trapping states that serves to facilitate rapid migration of space charge through the system. Clear parallels are evident here, as evinced by the abrupt transition from highly insulating (conductivity ~10^{-17} S/cm) in lightly aged samples (ageing times 0 – ~200 h) to relatively conducting (conductivity ~10^{-12} S/cm) in highly aged samples (ageing times >~250 h). As such, the data presented here reinforce our previous assertions of the critical role played by discrete deep traps, when present above a critical concentration, in facilitating conduction. However, the finding to emerge here that was not anticipated, is the apparent lack of influence of the spatial distribution of the crystalline phase. Contrast 124I/360 and 115I/360, for example: to a first approximation, the former system is composed of "discrete" isothermal crystalline inclusions dispersed within a "continuous" and defective (i.e. conducting) amorphous phase; the latter is composed of "discrete" defective (i.e. conducting) amorphous inclusions, separated by a "continuous" crystalline phase. While the terms continuous and discrete are used somewhat loosely here, variations in t_{at} between the different systems provides strong evidence for significant differences in the tortuosity of intra-amorphous diffusion paths. Despite this, the measured conductivity in all three systems saturates at an equivalent value. One interpretation of this is that the conduction process occurs in some equivalent manner in both the highly defective amorphous and non-defective crystalline regions. This appears implausible, both in view of the body of theoretical work contrasting change transport through crystalline and amorphous PE and due to experimental observations pointing to the importance of a critical concentration of defects in mediating charge transport, which cannot be present within the ordered structure of crystals. Based solely on the results presented here, further speculation on the mechanistic origins of this unexpected result is not warranted; a more detailed analysis of charge transport as revealed by a detailed analysis of dielectric relaxation processes, space charge dynamics and temperature dependent measurements of conductivity will be reported in due course.

6. Acknowledgments

The authors acknowledge the Electricity Generating Authority of Thailand and the University of Southampton for financial sponsorship. All data supporting this study are openly available from the University of Southampton repository at https://doi.org/10.5258/SOTON/D1234.

7. References

[1] 'ULTRANET – The energy transition in Germany-Siemens supplies converters technology to Amprion and TransnetBW for successful grid expansion', https://www.siemens.com/press/pool/de/feature/2016/energymanagement/2016-04-ultranet/presentation-ultranet-e.pdf, accessed 06 August 2018

[2] Gustafsson, A., Saltzer, M., Farkas, A., et al.: 'The new 525 kV extruded HVDC cable system: World´s most powerful extruded cable system'. ABB Grid Systems, 2014.
[3] Bergelin, P., Jeroense, M., Quist, T., et al.: '640 kV extruded HVDC cable system: World´s most powerful extruded cable system'. NKT, 2017.
[4] Ulf, N., Annika, S., Alfred, C.: 'The invention relates to a cable comprising a semiconductive layer and an insulation layer with improved DC electrical properties'. Austria Patent EP3190152A1, 2017.
[5] Peacock, A.: 'Handbook of polyethylene: structures, properties, and applications*'* (Marcel Dekker Inc., 2000)
[6] Bracco, P., Costa, L., Luda, M. P., et al.: 'A review of experimental studies of the role of free-radicals in polyethylene oxidation', *Polym. Degrad. Stab.,* 2018, 155, pp. 67-83
[7] Rapp, G., Tireau, J., Bussiere, P.-O., et al.: 'Influence of the physical state of a polymer blend on thermal ageing', *J. Polym. Degrad. Stab*., 2019, 163, pp. 161-173
[8] Hamzah, M., Khenfouch, M., Rjeb, A., et al.:, 'Surface chemistry changes and microstructure evaluation of low density nanocluster polyethylene under natural weathering: A spectroscopic investigation,' *J. Phys. Conf. Ser.*, 2018, 984, p. 012010
[9] Hamouya, M., Mahir, A., Idrissi, M. C. E.: 'Natural Ageing of Stabilized and Unstabilized LDPE Films Used as Greenhouses Covering Materials: ATR-FTIR and SEM Analysis', *Int. J. Res. Eng. Tech.*, 2014, 03, pp. 12-19
[10] Crine, J.-P.: 'Influence of high electrical fields on ageing and polarization properties of polyethylene', *J. Polym. Int.,* 2002, 51, pp. 1159-1163
[11] Wang, Y., MacKernan, D., Cubero, D., et al.: 'Single electron states in polyethylene', *J. Chem. Phys.,* 2014, 140, p. 154902
[12] Cubero, D., Quirke, N., Coker, D. F.: 'Electronic states for excess electrons in polyethylene compared to long-chain alkanes', *Chem. Phys. Lett.,* 2003, 370, pp. 21-25.
[13] Laurent, C., Teyssedre, G.: 'Energetics of charge transport in insulating polymers'. *Int. Symp. on Electrical Insulating Materials (ISEIM)*, 2017, pp. 3-9
[14] Meunier, M., Quirke, N., Aslanides, A.: 'Molecular modeling of electron traps in polymer insulators: chemical defects and impurities', *J. Chem. Phys.,* 2001, 115, pp. 2876-2881
[15] Wang, W., Tanaka, Y., Takada, T.: 'Space charge of polyethylene and electronic structure analysis of trapping site using common chemical groups' *Sens. Mater.,* 2017*,* 29, pp. 1223–1231
[16] Andersson, M. G., Hynynen, J., Andersson, M. R., et al.: 'Highly insulating polyethylene blends for high-voltage direct-current power cables', *ACS Macro Lett.,* 2017, 6, pp. 78-82
[17] Montanari, G. C., Seri, P., Lei, X., et al.: 'Next generation polymeric high voltage direct current cables—A quantum leap needed?', *IEEE Electr. Insul. Mag.,* 2018, 34, pp. 24-31
[18] Green, C. D., Vaughan, A. S., Stevens, G. C., et al: 'Thermoplastic cable insulation comprising a blend of isotactic polypropylene and a propylene-ethylene copolymer', *IEEE Trans. Dielectr. Electr. Insul.,* 2015, 22, pp. 639-648
[19] Tantipattarakul, S., Vaughan, A. S., T. Andritsch: 'On the influence of chemical defects and structural factors on charge transport and failure in polyethylene', *IEEE Trans. Dielectr. Electr. Insul.,* 2019, 27, pp. 259-266
[20] Tantipattarakul, S., Vaughan, A. S., T. Andritsch: 'On the influence of morphology and chemical defects on charge transport dynamics in polyethylene: thermal ageing and concentration gradient', *J. Phys. D: Appl. Phys.,* 2019, 52, p. 395302
[21] Bassett, D. C., Hodge, A. M., Olley, R. H.: 'On the morphology of melt-crystallized polyethylene II. lamellae and their crystallization conditions', *Proc. R. Soc. London A-Math. Phys. Sci.,* 1981, 377, pp. 39-60
[22] Hosier, I. L., Vaughan, A. S., Swingler, S. G.: 'Structure–property relationships in polyethylene blends: the effect of morphology on electrical breakdown strength', *J. Mater. Sci.,* 1997, 32, pp. 4523–4531
[23] Audouin, L., Langlois, V., Verdu, J., et al.: 'Role of oxygen diffusion in polymer ageing: kinetic and mechanical aspects', *J. Mater. Sci.,* 1994, 29, pp, pp. 569–583
[24] Lambert, J. B., Gronert, S., Shurvell, H. F., et al: 'Organic structural spectroscopy' (Pearson Prentice Hall, 2011, 2nd edn)
[25] Veitmann, M., Jumeau, R., Bourson, P., et al: 'Understanding and control of high temperature oxidation flaws of low-density poly(ethylene) with Raman spectroscopy', *Int. J. Spectr.*, 2014, pp. 1-9
[26] Teckoe, J., Bassett, D. C., Olley, R. H.: 'Aspects of the morphology and melting behavior of constrained polyethylene fibers', *Polym. J.,* 1999, 31, pp. 765-771
[27] ASTM: 'ASTM D257-14: Standard test methods for DC resistance or conductance of insulating materials', 2014
[28] Anandakumaran, K., Stonkus, D. J.: 'Assessment of oxidative thermal degradation of crosslinked polyethylene and ethylene propylene rubber cable insulation', *Polym. Eng. Sci.,* 1992, 32, pp. 1386-1393
[29] Winslow, F. H., Hellman, M. Y., Matreyek, W., et al.: 'Autoxidation semicrystalline polyethylene', *Polym. Eng. Sci.,* 1966, 6, pp. 273-278
[30] Carlsson, D. J., Lacoste, J.: 'A critical comparison of methods for hydroperoxide measurement in oxidized polyolefins', *Polym. Degrad. Stab.,* 1991, 32, pp. 377-386
[31] Sayers, P. W., Lewis, T. J., Llewellyn, J. P., et al.: 'Investigation of the structural changes in LDPE and XLPE induced by high electrical stress'. *Int. Conf. on Dielectric Materials, Measurements and Applications*, Edinburgh, UK, 2002, pp. 403-407
[32] Hosier, I. L., Vaughan, A. S., Swingler, S. G.: 'On the effects of morphology and molecular composition on the electrical strength of polyethylene blends," *J. Polym. Sci. B.: Polym. Phys.,* 2000, 38, pp. 2309–2322
[33] Vaughan, A. S., Stevens, G. C.: 'On crystallization, morphology and radiation effects in poly (ether ketone)', *Polym.*, 1995, 36, pp. 1531-1540
[34] Vaughan, A. S., Hosier, I. L.: 'The effect of dibenzylidene sorbitol on the crystallization behaviour of polyethylene', *J. Mater. Sci.,* 2008, 43, pp. 2922-2928
[35] Li, H., Li, J., Ma, Y., et al.: 'The role of thermo-oxidative aging at different temperatures on the crystal

structure of crosslinked polyethylene' *J. Mater. Sci.: Mater. Electr.,* 2018, 29, pp. 3696-3703
[36] Mattozzi, A., Neway, B., Hedenqvist, M. S., et al.: 'Morphological interpretation of n-hexane diffusion in polyethylene', *Polym.,* 2005, 46, pp. 929-938
[37] Zhao, B. and Zikry, M. A.: 'Oxidation-induced failure in semi-crystalline organic thin films', *Int. J. Solids Struct.,* 2017, 109, pp. 72-83
[38] Chmelař, J., Pokorný, R., Schneider, P., et al.: 'Free and constrained amorphous phases in polyethylene: Interpretation of 1H NMR and SAXS data over a broad range of crystallinity', *Polym.,* 2015, 58, pp. 189-198
[39] Khabbaz, F., Albertsson, A. C., Karlsson, S.: 'Chemical and morphological changes of environmentally degradable polyethylene films exposed to thermo-oxidation', *Polym. Degrad. Stab.,* 1999, 63, pp. 127-138
[40] Takahashi, S., Kiran, E.: 'Development of ring-banded spherulitic morphologies and formation of radially oriented nano-pores in poly(3-hydroxybutyrate-co-3-hydroxyvalerate) during crystallization in CO2', *J. Supercrit. Fluids.,* 2015, 96, pp. 359-368
[41] Olley, R. H.: 'Selective etching of polymeric materials', *Sci. Prog.,* 1986, 70, pp. 17-43
[42] Olley, R. H., Bassett, D. C., Vaughan, A. S., et al.: 'Delineating water trees in cross-linked polyethylene: a new technique', *J. Mater. Sci.,* 1992, 27, pp. 5192-5198
[43] Green, C. D., Vaughan, A. S., Stevens, G. C., et al.: 'Recyclable power cable comprising a blend of slow-crystallized polyethylenes' *IEEE Trans. Dielectr. Electr. Insul.,* 2013, 20, pp. 1-9
[44] Keith, H. D., Padden, F. J.: 'Banding in Polyethylene and Other Spherulites', *Macromolecules,* 1996, 29, pp. 7776-7786
[45] Lau, K. Y., Vaughan, A. S., Chen, G., et al.: 'Polyethylene/silica nanocomposites: absorption current and the interpretation of SCLC', *J. Phys. D: Appl. Phys.,* 2016, 49, p. 295305
[46] Ghorbani, H., Christen, T., Carlen, M., et al.: 'Long-term conductivity decrease of polyethylene and polypropylene insulation materials', *IEEE Trans. Dielectr. Electr. Insul.,* 2017, 24, pp. 1485-1493
[47] Shaw, A. V., Vaughan, A. S., Andritsch, T.: 'The effect of organoclay loading and matrix morphology on charge transport and dielectric breakdown in an ethylene-based polymer blend', *J. Mater. Sci.,* 2019, 54, pp. 13017-13028
[48] Hosier, I. L., Vaughan, A. S., Quirke, N.: 'Electrical conductivity of waxes as model systems for polyethylene: role of water', *J. Appl. Polym. Sci.*, 2019, 137, p.48765.
[49] Guo, T. C., Guo, W. W.: 'A transient-state theory of dielectric relaxation and the Curie-von Schweidler law', *J. Phys. C.: Solid State Phys.,* vol. 16, pp. 1955-1960, 1983.
[50] Karlsson, M. E., Xu, X., Hillborg, H., et al.: 'Lamellae-controlled electrical properties of polyethylene – morphology, oxidation and effects of antioxidant on the DC conductivity', *RSC Adv.,* 2020, 10, pp. 4698-4709
[51] McAloon, B. J., Perkins, P. G.: 'Semi-empirical LCAOMO theory for infinite systems. Part 1.—Application to polyethylene, polyacetylene and polyvinylchloride', *J. Chem. Soc., Faraday Trans. 2,* 1972, 68, pp. 1121-1132
[52] Süle, P., Kurth, S., Van Doren, V. E.: 'Orbital dependent exchange-only methods for periodic systems', *Phys. Rev. B.,* 1999, 60, pp. 5429-5439
[53] Moyassari, A., Unge, M., Hedenqvist, M. S., et al.: 'First-principle simulations of electronic structure in semicrystalline polyethylene', *J. Chem. Phys.,* 2017, 146, p. 204901
[54] Meunier, M., Quirke, N.: 'Molecular modelling of electron trapping in polymer insulators', *J. Chem. Phys.,* 2000, 113, pp. 369-376
[55] Cubero, D., Quirke, N.: 'Computer simulations of localized small polarons in amorphous polyethylene', *J. Chem. Phys.*, 2004, 120, pp. 7772-7778
[56] Boukezzi, L., Rondot, S., Jbara, O., et al.: 'A time-resolved current method and TSC under vacuum conditions of SEM: trapping and detrapping processes in thermal aged XLPE', *Nucl. Instrum. Meth. B*, 2017, 394, pp 126-133